INTERNATIONAL SOCIETY FOR SOIL MECHANICS AND GEOTECHNICAL ENGINEERING

SIMSG | ISSMGE

COMPARISON OF FREQUENCY AND TIME-DOMAIN OBJECTIVE FUNCTIONS FOR BOREHOLE STATION'S INVERSE PROBLEMS

Florent DE MARTIN[1]

ABSTRACT

This paper compares the use of frequency and time-domain objective function for the inversion of the soil structure using borehole station data. It is shown that the length of the cosine-shaped window used to taper the time history to be transformed by the Fast Fourier Transform influences the global shape of the spectral ratios (i.e., both frequency and amplitude of the resonant frequencies of the soil column are affected by the length of the cosine-shaped window). Consequently, the inversions using frequency-domain objective function are distorted by the length of the cosine-shaped windows that is generally chosen arbitrarily between 15 and 50% of the length of the S-wave portion. In order to avoid this effect, this paper introduces a time-domain objective function that computes the integrated residual between a simulated time history and the raw observation. The results show that the match of the simulated time histories with the observation is better when the time-domain objective function is used.

Keywords: borehole, inversion, objective function, 1D simulation, sedimentary basin, earthquake

INTRODUCTION

The quantification of local site effects on seismic ground motions is of great importance in earthquake engineering in order to better evaluate the seismic hazard. In the frequency range of interest of the earthquake engineering structures, the most practical approach to quantify local site effects is the one-dimensional (1D) theory that mainly rely on the soil layers properties as the shear-wave (S-wave) velocity and the damping factors.

In order to corroborate or adjust the soil properties obtained by geotechnical or geophysical methods in the low-strain range, inversion methods using small aftershocks data from vertical arrays are now widely used and have shown their efficiency to improve aftershocks simulations (e.g., Satoh et al., 2001; Assimaki and Steidl, 2007). Vertical arrays data recorded during strong ground motions can be used as well to quantify the empirical equivalent linear properties of the soil structures (e.g., Satoh et al., 1995b; Kokusho, 2004; De Martin et al., 2010).

For the inversion of the S-wave velocity and damping factors, a common objective function is the computation of the integrated residuals between an observed spectral ratio and a theoretical one computed by the 1D theory (e.g., Satoh et al., 1995a). In order to isolate the S-wave portion (i.e., in order to avoid including the P and coda waves that could alter the observed S-wave spectral ratio) a cosine-shaped window is applied around the S-wave portion to make the signal causal at both ends for the computation of the Fast Fourier Transform (FTT). This application of the cosine-shaped window is a shortcoming of the process of the inversion methods because the inclusion of a certain quantity of P and coda waves

---

[1] Dr., Natural Risks and CO_2 Storage Safety Division, brgm, France, e-mail: f.demartin@brgm.fr

(even smoothed by a cosine-shaped window) modifies the S-wave portion of the downhole and free surface signals and consequently their FTT and the final spectral ratio. In practice, the length of the cosine-shaped windows is fixed as a percentage of the length of the S-wave portion. Common values range (as a rule of thumb) between 15% and 50% and one can shown that for such a range, the spectral ratios differ: the location of the resonant peaks along the frequency axis can be slightly affected and the amplitude of the peaks can be greatly affected. As a result, the inversion of the S-wave velocity and damping factors can be distorted because of the application of the cosine-shaped window.

The objective of this paper is to introduce a simple time-domain objective function for borehole data inversion methods and to compare the results of inversions by using either frequency or time-domain objective functions. First, the borehole station and the data used in this study are presented. Then, the influence of the cosine-shaped window on S-wave spectral ratios is shown for several aftershocks. Finally, the soil layers properties are inverted using a genetic algorithm (GA) code (e.g., Demartin et al., 2010). To show the robustness of the inversions present in this paper, for each inversion, eight independent inversions are performed so that a mean and a standard deviation can be shown.

OVERVIEW OF THE BOREHOLE STATION AND ITS DATA

The borehole station of this study (lon/lat =138.609341°E/37.427328°N) is the Kariwa Service Hall (KSH) station installed on the Kashiwazaki-Kariwa nuclear power plant site of Tokyo Electric Power Company (TEPCO). The borehole station is composed of four acceleration sensors (called SG1 to SG4) with a sample frequency of 100 Hz installed at 2.4 m depth (SG1), 50 m depth (SG2), 100 m depth (SG3) and 250 m depth (SG4).

The soil layers properties along the borehole provided by Tokyo Electric Power Company (2008) are presented in Table 1 and plotted in Figure 1. The KSH vertical array is located on the Arahama sand dune. The first 15.5 m are composed of recent sand deposit from the Holocene with a S-wave velocity ranging from 40 to 230 m/s, then follows the Banjin formation (a late Pleistocene sand deposit) until 71 m depth with a S-wave velocity ranging from 280 to 390 m/s. Below, the Yasuda formation (a late Pleistocene clay deposit) is present until 83 m depth with a S-wave velocity ranging from 330 to 390 m/s and then follows the Nishiyama formation (bedrock of mudstone from early Pleistocene) until the downhole with a S-wave velocity ranging from 490 to 650 m/s.

Table 1. Soil layers properties at the KSH station provided by Tokyo Electric Power Company (2008).

| Soil classification	No.	Thickness (m)	S-wave velocity (m/s)	Density (t/m^3)
Recent sand deposit	1	2.4	40	1.57
	2	2.0	120	1.57
	3	4.0	150	1.57
	4	7.1	230	1.57
	5	14.5	280	1.57
Banjin formation	6	15.0	330	1.57
	7	26.0	390	1.65
Yasuda formation	8	12.0	490	1.65
Nishiyama formation	9	87.0	550	1.64
	10	35.0	600	1.67
	11	∞	650	1.74
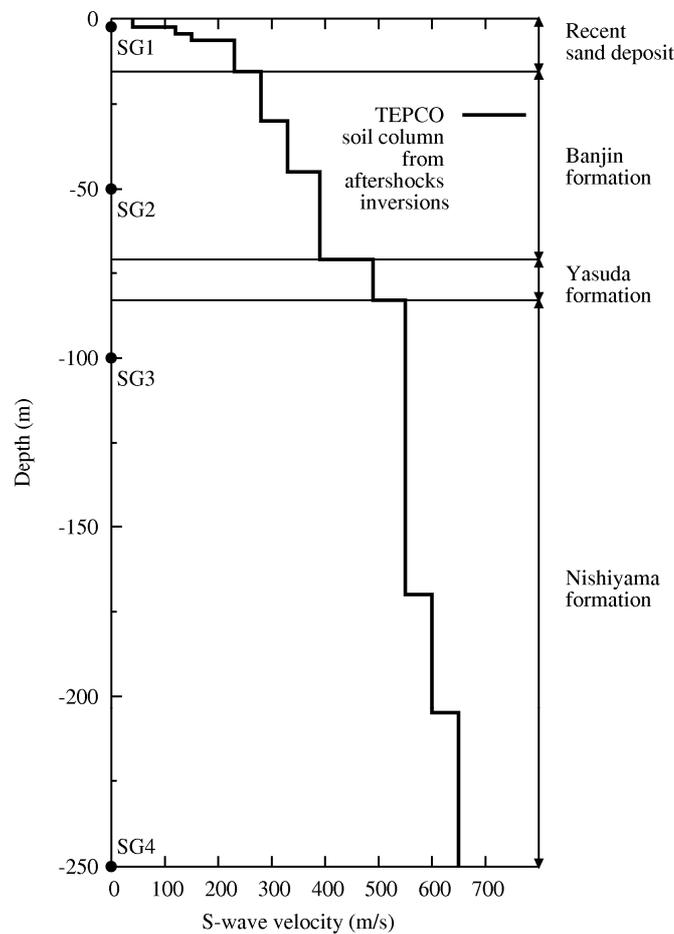
Figure 1. Soil profile at the KSH site provided by TEPCO (2008). The sensors SG1 to SG4 are represented by dots on the vertical axis

The epicenter of the earthquakes recorded between July 2007 and August 2007 by the borehole station is presented in Figure 2. Characteristic of earthquakes determined by the JMA are shown in Table 2.

In the following, spectral ratios are computed by using different cosine-shaped windows in order to show their influence on the global shape of the spectral ratios.

Table 2. List of earthquakes whose parameters are determined by the JMA

No.	Date YY.MM.DD/HH:MM	Lon./Lat.	Focal depth (km)	Magnitude
EQ01	07.07.16/10:13	37.55667/138.60833	17	6.8
EQ02	07.07.16/11:00	37.45667/138.56500	22	3.7
EQ03	07.07.16/15:37	37.50333/138.64333	23	5.8
EQ04	07.07.16/17:42	37.41333/138.55667	19	4.2
EQ05	07.07.16/21:08	37.50833/138.62833	20	4.4
EQ06	07.07.25/06:52	37.53167/138.72000	24	4.8
EQ07	07.08.04/00:16	37.42000/138.53667	18	3.2
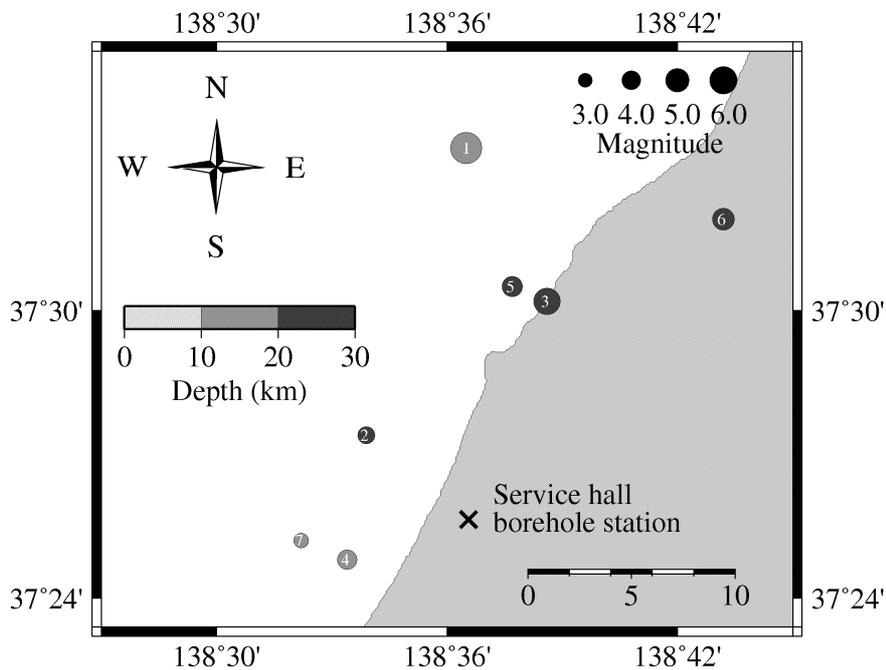
Figure 2. Epicenter of the earthquakes used in this study. The borehole station is indicated by a cross. Numbers inside each epicenter correspond to the earthquake number of Table 2.

INFLUENCE OF THE LENGTH OF A COSINE-SHAPED WINDOW ON S-WAVE SPECTRAL RATIOS

Because of the presence of four sensors along the borehole, different choices of spectral ratios can be made. In order not to inverse too much parameters in the next section, the spectral ratios SG1/SG3 have been chosen. We note that the spectral ratio SG1/SG2 could have been chosen but the resonant frequencies were not as clear as the ones on the ratios SG1/SG3. The ratios SG1/SG4 also exhibit nice resonant frequencies, however, the number of parameters to invert increase. The ratios SG1/SG3 are therefore a good trade-off between the quality of spectral ratios and the number of parameters to invert. We also note that only the results obtained on the radial direction are shown in this paper.

An example of cosine-shaped signals in the time domain for EQ07 is shown in Figure 3. The S-wave portion has been chosen so that the incoming S-wave (around 11.1 sec at SG3) and its free surface reflection (around 11.8 sec at SG3) are included in the signal at SG3. We note that due to the small magnitude (3.2) of EQ07, the assumed S-wave portion is short (only 1.53 s). For earthquakes with larger magnitude, the length of S-wave portion is generally larger (about 3 s to 5 sec).

In order to compute the spectral ratios, the FFT is performed on time histories of 40.96 s and a Parzen spectral window of bandwidth 0.1 Hz is used to smooth the ratios. Figure 4 shows the influence of the length of the cosine-shaped windows on the spectral ratios SG1/SG3 for different earthquakes. The length of the cosine shape slightly affects the location of the resonant peaks along the frequency axis and strongly affects the amplitude of the peaks. For instance, for EQ02, the amplitudes of the second mode (located around 2.2 Hz) are 46.7, 19.5, 11.3 and 9.5 for cosines shape of 15%, 25%, 35% and 45%,

respectively. As a result, the inversion of the damping factors or the S-wave velocity can be distorted due to the application of the cosine-shaped window of an arbitrary length.

Besides, we note that the resonant frequencies observed for EQ02 and EQ07 match very well up to the 5th resonant frequency. The fundamental mode is around 0.9 Hz, the second mode around 2.2 Hz, the third mode around 3.5 Hz, the fourth mode around 5.2 Hz and the fifth mode around 6.4 Hz. This good stability can be found using other aftershocks and suggests that these resonant modes are the modes of the soil column between SG1 and SG3 in the linear domain. As for EQ03, we note a clear shift toward the low-frequency range of the modes two and four. This shift is probably due to the nonlinear behavior of soft soils during EQ03 for which the PGAs recorded at the free surface are 162 cm/s and 186 cm/s in the NS and EW directions, respectively (cf. Table 3). Figure 4 also shows the 1D theoretical transfer function between SG1 and SG3 plotted together with EQ07. We can clearly see that the soil column of Table 1 overestimate the observed resonant modes and consequently, overestimate the S-wave velocity of the soil layers. As a result, the search space of the inversions performed in the following section will be reduced to S-wave velocity inferior or equal to those shown in Table 1.

Table 3. PGA in cm.s^{-2} in the NS, EW and UD directions at the sensor SG1 of the station KSH

| No.	NS	EW	UD
EQ01	347.2	437.3	590.3
EQ02	35.8	22.9	45.2
EQ03	162.5	186.2	193.6
EQ04	34.9	50.0	36.8
EQ05	73.2	51.3	66.3
EQ06	64.4	76.6	48.9
EQ07	18.1	32.5	26.3

FREQUENCY AND TIME-DOMAIN INVERSIONS OF THE SOIL STRUCTURE BY GENETIC ALGORITHM

In order to refine the 1D soil column between the sensors SG1 and SG3 so that the theoretical resonant frequencies match the observed ones, both frequency and time-domain inversions are performed to optimize the S-wave velocity and the damping factors. The objective function for the frequency-domain inversions is presented in Equation 1.

$$E(\mathbf{x}) = \frac{\int_{f_s}^{f_e} |H_o(f) - H_t(f, \mathbf{x})|^2 df}{\int_{f_s}^{f_e} |H_o(f)|^2 df}, \tag{1}$$

where E is the objective function, $\mathbf{x}$ the vector of unknown parameters, f the frequency, f_s and f_e the start and end frequencies of integration, H_o the observed spectral ratio and H_t the theoretical spectral ratio. The objective function in the time domain is simply the absolute value of the difference between the observed and theoretical acceleration time histories as expressed in Equation 2.

$$E(\mathbf{x}) = \int_{t_s}^{t_e} |A_o(t) - A_t(t, \mathbf{x})| dt, \tag{2}$$
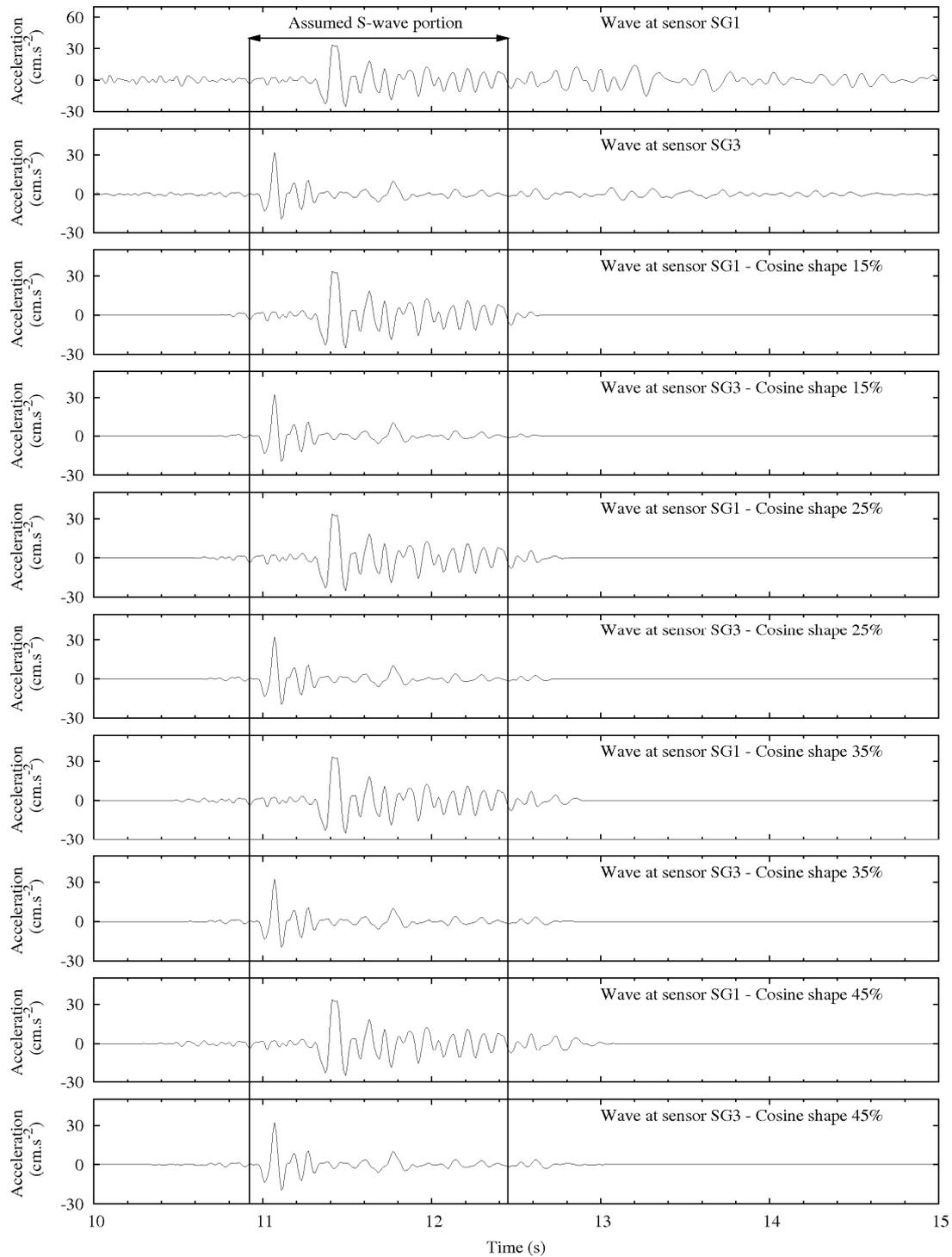
Figure 3. Recorded waves and cosine-shaped waves at the sensors SG1 and SG3 during EQ07. The assumed S-wave portion is indicated by a horizontal arrow (the last part of the record is supposed to be coda waves that are not taken into account by the 1D theory). The cosine-shaped windows are applied outside both ends of the S-wave portion. The length of the cosine shape is indicated inside each panel as a percentage of the length of S-wave portion.
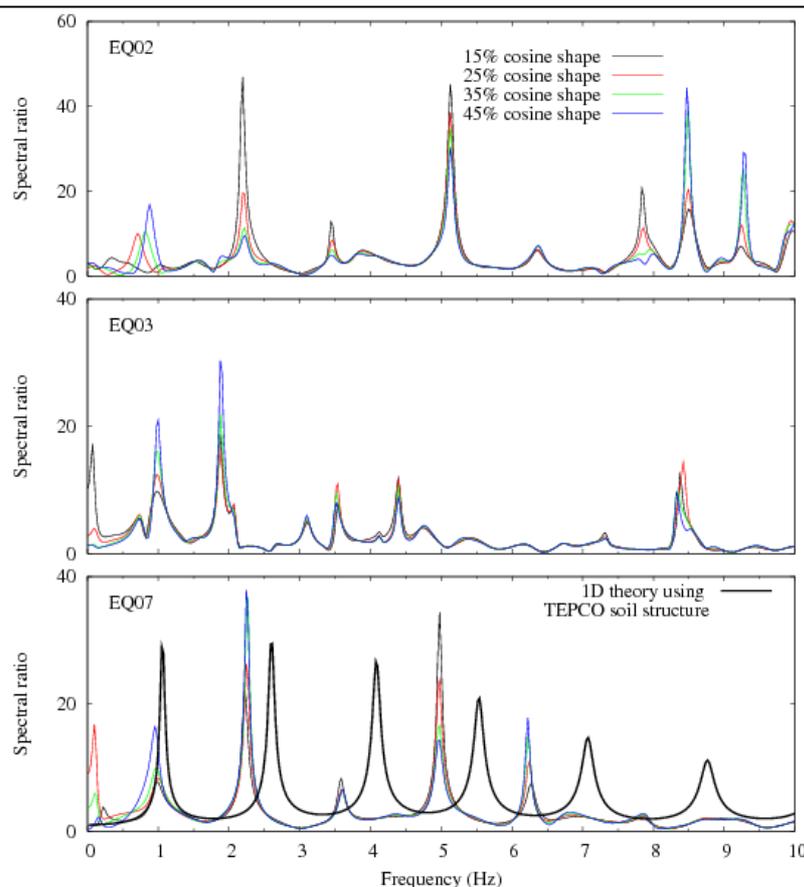
Figure 4. Influence of the length of different cosine-shaped windows on the spectral ratio of EQ02, EQ3 and EQ07. The lengths of the cosine-shaped windows are 15%, 25%, 35% and 45% of the assumed S-wave portion. The 1D theory using S-wave velocity of Table 1 is plotted together with the spectral ratio of EQ07 (a constant arbitrary damping factor of 1% as been used on the entire soil column).

where t is the time, t_s and t_e the start and end time of integration, A_o the observed acceleration time history and A_t the theoretical one.

For all the frequency and time-domain inversions, the genetic algorithm parameters are the same (a detailed explanation of the process of the inversion by GA performed in this paper is given in Demartin2010). Prior to the GA inversion, a Monte Carlo search is performed over 20 populations of size 4096 individuals in order to explore the search space. The best 1024 individuals found during the Monte Carlo search are used to generate the first GA population. One GA inversion runs over 4000 populations of size 1024 individuals. Probability of uniform crossover and mutation are 85% and 0.1%, respectively. The selection of the parent individuals is done by tournament of size 5 individuals. Elitism is activated so that the best 10 individuals are always present in the populations.

Both S-wave velocity and damping factors of each layer between the sensors SG1 and SG3 are inverted (the layers 2 and 3 have been merged so that the total number of layers between SG1 and SG3 is 8). The damping factors are frequency independent. The S-wave velocity is searched in the space [0.5-1.0] times the S-wave velocity of Table 1. The damping factors are searched in the space [0-50%]. The discretization of each inverted parameter is done using 6 bytes (i.e., 2^6=64 discrete values). Thus, the total

number of possible solution for an inversion is $2^{8 \times 2 \times 6}=7.9 \times 10^{28}$. In order to guarantee the convergence of an inversion to a possible global minimum, 8 independent inversions are performed so that the mean and standard deviation of the S-wave velocity and damping factors can be computed. A small standard deviation guarantees the convergence to a possible global minimum.

The EQ07 has been chosen for the inversion. The frequency and time-domain inversions use the S-wave portion of EQ07 shown in Figure 3. The frequency-domain inversion is performed up to 10 Hz and the time-domain inversion is performed on Butterworth low-pass filtered wave with a corner frequency of 10 Hz. The frequency-domain inversions on the spectral ratios computed by using the cosine-shaped windows of length 15%, 25%, 35% and 45% are shown in Figure 5. The spectral ratios found by the 8 independent time-domain inversions are shown in the same figure. The corresponding soil structures and simulated time histories are shown in Figure 6 and Figure 7, respectively. We note that the simulated time histories are obtained by convolution of the entire record at SG3 with the theoretical transfer function obtained by inversion (even if only the assumed S-wave portion is supposed to be governed by the 1D theory).
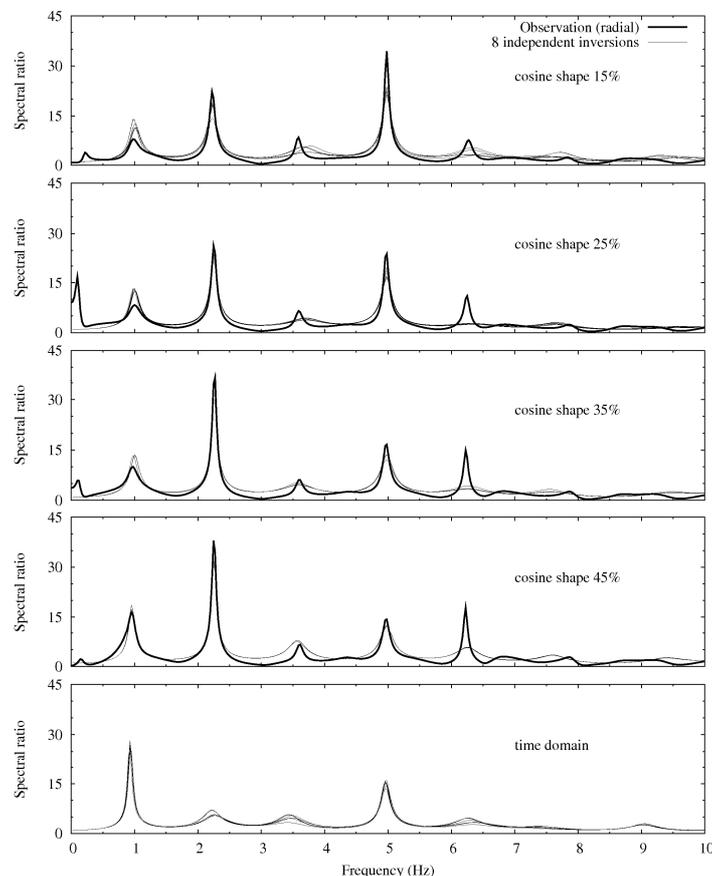
Figure 5. Panels 1 to 4: frequency domain inversions of EQ07. The inverted spectral ratios are plotted together with the observed one computed by using a cosine-shaped windows of 15%, 25%, 35% and 45%, respectively. The inversions have been performed in the frequency range 0.2-8.0 Hz. Panel 5: time domain inversion of EQ07. No observed spectral ratio is plotted since the inversion is done on the time history.
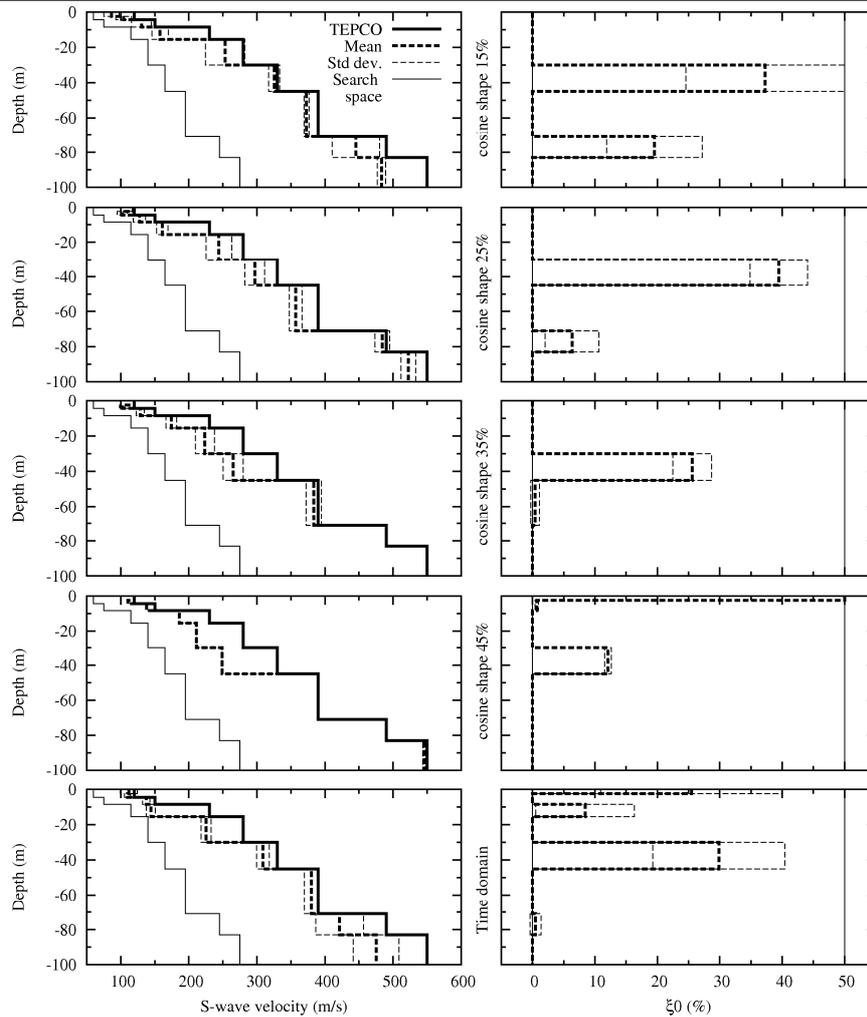
Figure 6. Left panels 1 to 4: mean and standard deviation of the inverted S-wave velocity found by the frequency-domain inversions for cosine-shaped windows of length 15% to 45%. Left panel 5: mean and standard deviation of the inverted S-wave velocity found by the time-domain inversions. Right panels: inverted damping factors corresponding to the left panels.

As for the frequency-domain inversions, the inverted spectral ratios match well the observed ones. The discrepancy of peaks amplitude caused by different length of cosine-shaped windows is fairly well reproduced by the theory; this means that the effect of the length of the cosine shape is, as expected, included in the inverted S-wave velocity and damping factors. This effect can be seen in Figure 6 where different S-wave velocity and damping factors are found for different length of cosine-shaped windows.

As for the time-domain inversions, we can see in Figure 5 that the 1D resonant frequencies are found even if the objective function is based on the time history. In terms of S-wave velocity and damping factors, we can see in Figure 6 that the frequency-domain inversion with a 35% cosine-shaped window is the closest to the structure inverted in the time-domain. For some layers, we note unexpected large damping factors for both frequency and time-domain inversions. However, prior inversions were performed searching the damping factors in the interval [0-15%] but the upper bound 15% were reached for the layers that have large damping factors in the inversions show in this paper. These large damping

factors might be explained by the fact that the sensor located at 2.4 meters depth has been placed at the free surface during the inversion.

As for the simulated time history shown in Figure 7, the bias induced by the length of the cosine-shaped windows is visible for the simulated time histories coming from the inversion performed in the frequency domain. As for the simulated time history using the time-domain objective function, the result is much better. The fit is almost perfect on the entire assumed S-wave portion. Moreover, after examination of the particle orbit of the acceleration in the vertical plane at the sensor SG1 and SG3, we see that the deviation of the 1D theory with the observation at 12 sec in Figure 7 may correspond to the arrival of surface wave shown in Figure 8 where the particle orbit becomes complex at SG1 and SG3 after 12 sec.
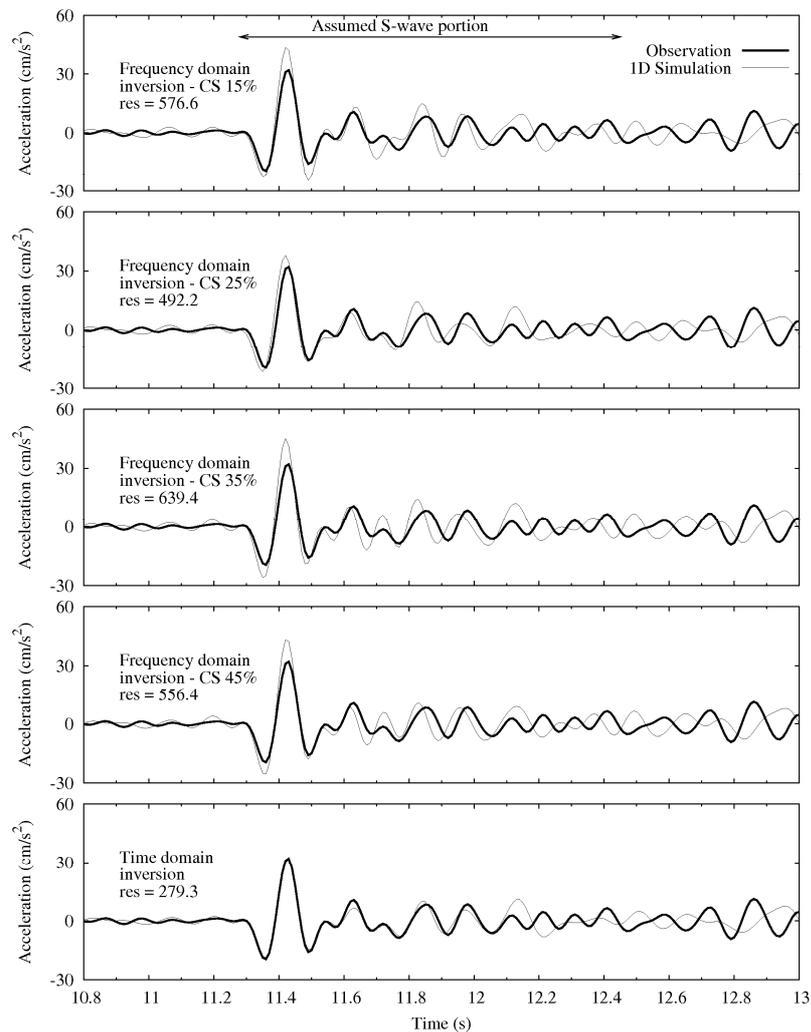
Figure 7. Panels 1 to 4: observed and simulated time history using the frequency domain inversions for cosine-shaped windows of length 15% to 45%. Panel 5: observed and simulated time history using the time domain inversions. The result of Equation (2) is indicated by the variable "res" on each panel. The S-wave portion on which the inversions have been performed is indicated on the top of the first panel.

Particle orbit at SG1

Particle orbit at SG3
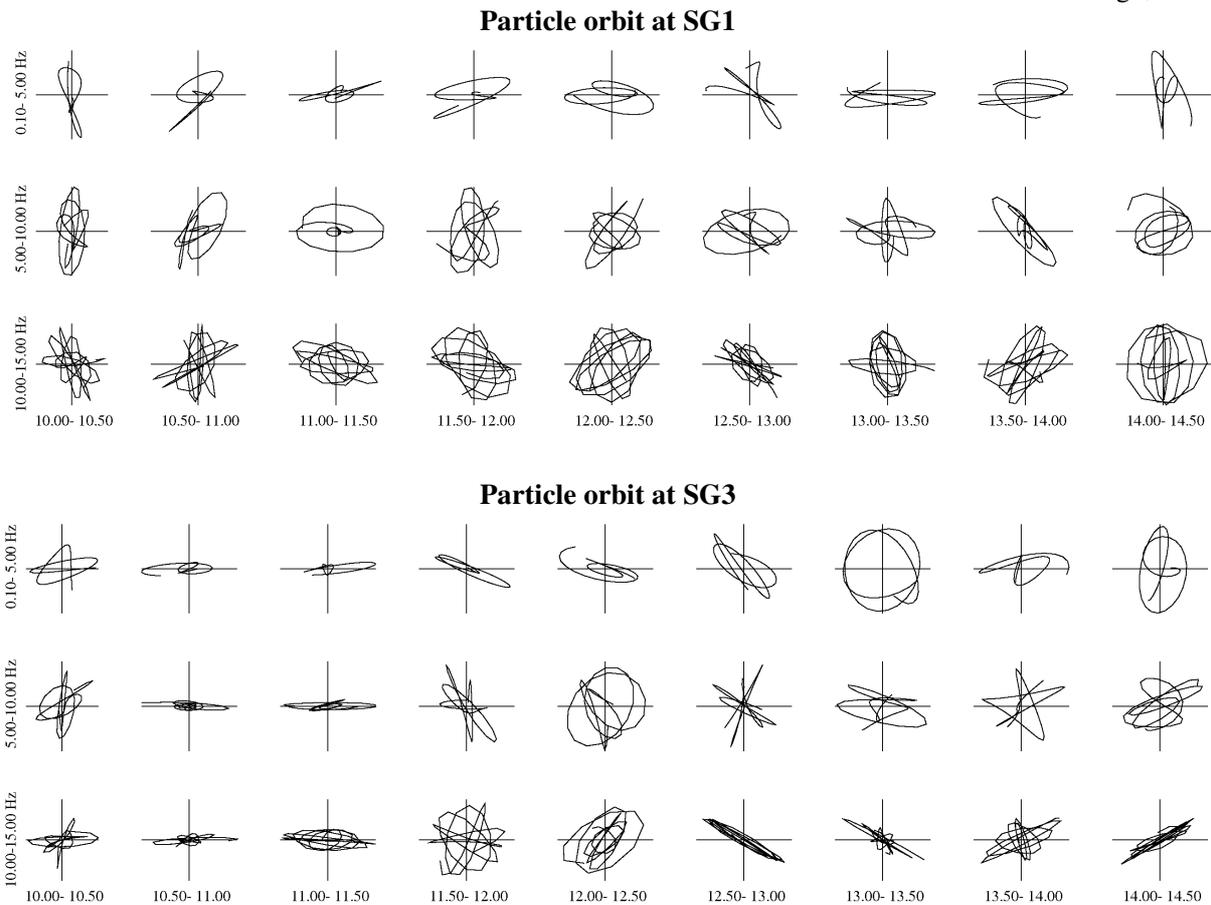
Figure 8. Particle orbit of EQ07 in the vertical plane plotted every 0.5 sec obtained using Butterworth band-pass filtered acceleration time history. The band-pass filter is indicated on the left-hand side. The time windows are indicated at the bottom and correspond to the absolute time of the previous figures plotted in the time domain. First three lines: particle orbit at SG1. Three bottom lines: particle orbit at SG3.

CONCLUSIONS

We have investigated the use of frequency and time-domain objective functions to invert borehole data. We have shown that the length of the cosine-shaped windows used to make the time history causal to perform the FFT is mapped into the global shape of the spectral ratios. Consequently, the inverted S-wave and damping factors are distorted according to the length of the cosine-shaped windows. A solution to avoid this distortion is to evaluate the soil structure in the time domain by using a time-domain objective function. We have shown that this technique gives the best results for the simulated time history and is accurate to find the resonant frequency of the soil column in the frequency domain.

ACKNOWLEDGEMENTS

REFERENCES

Assimaki, D. and J. Steidl (2007). Inverse analysis of weak and strong motion downhole array data from the Mw7.0 Sanriku-Minami earthquake. Soil Dynamics and Earthquake Engineering Vol. 27, No. 1, pp.73-92.

De Martin, F., H. Kawase, and A. Modaressi (2010). Nonlinear soil response of a borehole station based on one-dimensional inversion during the 2005 West off Fukuoka Prefecture earthquake. Bull. Seism. Soc. Am. Vol. 100, No. 1, pp 151-171.

Kokusho, T. (2004). Nonlinear site response and strain-dependent soil properties. Current Science Vol. 87, No. 10, pp. 1363-1369.

Satoh, T., M. Fushimi, and Y. Tatsumi (2001). Inversion of strain-depend nonlinear characteristics of soils using weak and strong motions observed by borehole sites in Japan. Bull. Seism. Soc. Am. Vol. 91, No. 2, pp. 365-380.

Satoh, T., H. Kawase, and T. Sato (1995a). Evaluation of local site effects and their removal from borehole records observed in the Sendai region, Japan. Bull. Seism. Soc. Am. Vol. 85, No. 6, pp. 1770-1789.

Satoh, T., T. Sato, and H. Kawase (1995b). Nonlinear behavior of soil sediments identified by using borehole records observed at the Ashigara valley, Japan. Bull. Seism. Soc. Am. Vol. 85, No. 6, pp. 1821-1834.